GERMAIN, G., MAIN, P. & WOOLFSON, M. M. (1970). *Acta Cryst.* B26, 274–285.

GERMAIN, G., MAIN, P. & WOOLFSON, M. M. (1971). *Acta Cryst.* A27, 368–376.

HAUPTMAN, H. & KARLE, J. (1959). *Acta Cryst.* 12, 846–850.

HAUPTMAN, H. & KARLE, J. (1962). *Acta Cryst.* 15, 547–550.

KARLE, J. & HAUPTMAN, H. (1964). *Acta Cryst.* 17, 392–396.

McCORMICK, I. R. N., NIXON, P. E. & WATERS, T. N. (1976). *Tetrahedron Lett.* (1976). 20, 1735–1736.

Optical Selected-Area Diffraction Patterns of High-Resolution Electron-Microscope Images for Crystal Analysis

BY T. TANJI AND H. HASHIMOTO

Department of Applied Physics, Osaka University, Suita 565, Japan

Optical selected-area diffraction patterns made from high-resolution electron micrographs of crystals have been used as a source of diffraction information from areas as small as a single unit cell of the crystal. The intensities of the electron diffraction pattern of the specimen crystal and the optical diffraction patterns of high-resolution electron-microscope images have been discussed by electron optical image formation theory taking account of spherical aberration and defocusing of the objective electron lens and it is concluded that the optical diffraction pattern may be identical with the electron diffraction pattern if the electron micrograph is photographed under optimum conditions. Optical diffraction patterns from areas of 80, 30 and 10 Å in diameter of labradorite feldspar have been taken and the orientation of two adjoining grains, 30 Å in diameter, has been determined. The diffraction pattern from a unit-cell area has also been taken and compared with the calculated intensity.

1. Introduction

The selected-area diffraction technique in electron microscopy serves to provide a diffraction pattern from a small finite area of a crystalline specimen under electron-microscope observation and can be used for identifying materials. Since, however, the objective lens of the electron microscope has a certain amount of spherical aberration, some diffracted beams from the region adjoining the field-limiting aperture can pass through the objective aperture and therefore influence the diffraction pattern. The error of correspondence between the specimen area selected and the area actually producing the diffraction pattern is expressed by $C_s \alpha^3$ as Riecke (1961) has shown, where α is the scattering angle of the electron waves and C_s is the spherical aberration coefficient of the objective lens. For example, when the diffraction pattern of a lattice plane with 1·13 Å spacing (Al_{222}) is taken at 100 kV with a lens having a spherical aberration coefficient $C_s = 3·6$ mm, the error in the selected specimen area is 1260 Å. Therefore, the correspondence between image and diffraction pattern will not hold if the area limited by the field aperture is small. However, for accurate structure analysis, the uncertainty in the correspondence should be avoided.

Uyeda, Dupouy, Perrier, Ayroles & Bousquet (1963) have pointed out that the error of the area limited by the field-limiting aperture becomes small at high voltages because then the scattering angle α for the electrons is small. Making use of this relation, Koreeda, Okamoto, Shimizu & Katsuta (1971) have shown that the minimum accurate area for taking the diffraction pattern of lattice planes with 1·0 Å spacing at 500 kV becomes 80 Å and diffraction patterns may be taken from an area 250 Å in diameter for crystals containing precipitates and lattice imperfections. Koike & Ueno (1973) and Geiss (1975) have used a small probe of the scanning transmission electron microscope to take diffraction patterns from areas as small as 50 Å in diameter of crystalline materials. Since in these techniques the field-limiting aperture limits the intensity of the electron beams which form the electron diffraction pattern, exposures of 1 to 5 min or more are necessary to take diffraction patterns. During these long exposures radiation damage, specimen contamination and drift of the specimen occur and thus there may be poor correspondence between image and diffraction

pattern. It is, therefore, preferable to take the diffraction pattern with as small an exposure time as possible, even in high-voltage electron microscopes and scanning transmission electron microscopes. Recently it has been shown by Allpress, Sanders & Wadsley (1968), Iijima (1971, 1973) and Uyeda, Kobayashi, Suito, Harada & Watanabe (1972) that high-resolution electron-microscope images of very thin crystals with large unit cells, taken at optimum focus by using many diffracted beams, show contrast patterns on the atomic scale very similar to the projected potential of the crystal lattice. Thon (1966) and Erickson & Klug (1971) have shown that the optical diffraction pattern of a high-resolution electron-microscope image of amorphous material shows the spatial frequency of the recorded image. Hashimoto, Tanji, Ono & Kumao (1975) have shown briefly that crystal lattices of labradorite feldspar can be studied from the optical diffraction pattern of its high-resolution electron-microscope images. Clarke & Thomas (1976) and Gronsky, Sinclair & Thomas (1976) have applied this technique to the study of the structure of ceramics and metals.

In the present paper, it will be discussed theoretically and experimentally how optical selected-area diffraction patterns made from high-resolution electron micrographs of crystals taken at suitable optimum focus can be used as a source of diffraction information from very small crystal areas down to the area of a single unit cell of the crystal. Some examples of orientation determination of labradorite feldspar and the accuracy of the selected area in this technique will also be shown.

2. Theory

The phase-grating approximation for the specimen crystal and electron optical image formation theory are applied to study the relation between the electron diffraction pattern and the optical diffraction pattern obtained from the electron micrograph of the specimen crystal. In very thin objects the electron wave may be considered to travel straight through the object undergoing only a phase change proportional to the electrostatic potential in the object (Cowley, 1959). The object is thus a phase object with transmission function

$$f(x,y) = \exp[-i\sigma\varphi(x,y)], \qquad (1)$$

where σ is the interaction constant ($\sigma = \pi/\lambda E$, λ is the electron wavelength and E is accelerating potential) and $\varphi(x,y)$ is the projection of the three-dimensional potential distribution of the specimen. For thin specimens consisting of light atoms, it can be assumed that the phase angle $\sigma\varphi$ is very much smaller than $\pi/2$ and (1) may be written

$$f(x,y) \simeq 1 - i\sigma\varphi(x,y). \qquad (2)$$

The amplitude $Q(u,v)$ of the electron diffraction pattern appearing in the back-focal plane of the objective lens is expressed by the Fourier transform of (2):

$$Q(u,v) = \delta(u,v) - i\sigma \mathscr{F}[\varphi(x,y)] \exp[-i\gamma(u,v)], \qquad (3)$$

where $uf\lambda$, $vf\lambda$ are coordinates in the back-focal plane, and f is the focal length of the lens; $\gamma(u,v)$ is the perturbation of phase due to defocus Δf and spherical aberration coefficient C_s of the lens and is written, after Scherzer (1949),

$$\gamma(u,v) = (\pi/2)[C_s\lambda^3(u^2 + v^2)^2 - 2\Delta f\lambda(u^2 + v^2)]. \qquad (4)$$

The intensity of the electron diffraction pattern is given from (3) as

$$I(u,v) = \delta(u,v) + \sigma^2\Phi^2(u,v), \qquad (5)$$

where $\Phi(u,v) = \mathscr{F}[\varphi(x,y)]$. The amplitude in the image plane is given by the Fourier transform of (3) as

$$\psi(x_i,y_i) = 1 - \mathscr{F}[\sigma\Phi(u,v) \sin \gamma(u,v)] \\ - i\mathscr{F}[\sigma\Phi(u,v) \cos \gamma(u,v)]. \qquad (6)$$

The intensity of the electron-microscope image is expressed as

$$I(x_i,y_i) = 1 - 2\sigma\varphi(-x_i, -y_i)_* \mathscr{F}[\sin \gamma(u,v)], \qquad (7)$$

where $*$ denotes a convolution operation and $|\sigma\varphi(x,y)|^2$ is neglected. It is seen in (7) that if $\sin \gamma(u,v)$ were equal to ± 1, the image contrast would be proportional to the projected potential $\varphi(x,y)$. It is known that blackening of a photographic plate varies linearly with electron beam intensity over a wide range. If the range of blackening is not too great, the amplitude of light transmitted by the plate is then linearly related to the incident electron beam intensity to a good approximation. When the optical diffraction pattern of the electron microscopic images is recorded on photographic film, considering the symmetry of $\Phi(U,V)$ and $\gamma(U,V)$, the amplitude of the diffraction pattern is given by the Fourier transform of (7) as

$$P(U,V) = \delta(U,V) - 2\sigma\Phi(U,V) \sin \gamma(U,V), \qquad (8)$$

where $UF\Lambda$, $VF\Lambda$ are the coordinates in the plane where the electron optical diffraction pattern is observed, Λ and F are the wavelength of the light and the focal length of the lens, respectively. When the selected area is limited, the well-known Fourier transform of the aperture function

$$\frac{\sin a\pi U}{\pi U} \frac{\sin b\pi V}{\pi V} \qquad (9)$$

should be convoluted with the diffraction pattern amplitude, where a and b are the lengths of the rectangular aperture.

The intensity of the optical diffraction pattern is given from (8) as

$$L(U,V) = \delta(U,V) + 4\sigma^2\Phi^2(U,V) \sin^2 \gamma(U,V). \qquad (10)$$

By comparing (5) and (10), it is easily seen that these equations are identical if σ in (5) is replaced by 2σ and the second term of (5) is multiplied by $\sin^2 \gamma(U,V)$. Therefore, the difference in contrast between the electron diffraction pattern and the optical diffraction pattern is in the $\sin^2 \gamma(U,V)$ in the second term of (10). Therefore, provided that the electron-microscope image is recorded in the optimum focus condition, where $|\sin \gamma(U,V)|$ is nearly equal to 1 in the wide range of space frequency, the intensity of the optical diffraction pattern of the recorded image is identical with that of the electron diffraction pattern. Even when the image is recorded in another focusing condition, it is possible to correct the obtained optical diffraction pattern to give one identical with the electron diffraction pattern by using the value $\sin^2 \gamma(U,V)$.

It should be remembered that the phase-object approximation (1) is valid only for very thin crystals. The upper limit of thickness for which it can be used varies with the wavelength and resolution. For present-day high-resolution microscopes it is about 50 Å. Also the further approximation of a weak phase object (2) can be used only for thin crystals with a limiting thickness, which depends mostly on the atomic numbers of the atoms present. It fails for a single layer of very heavy atoms but may be valid for crystal thicknesses up to about 100 Å for light atoms. In the next section we show clear evidence that the optical diffraction intensities can change strongly with crystal thickness. A detailed discussion based on a more complete theory of electron diffraction will be given elsewhere but it can be concluded that, within well-defined limitations, the optical diffraction patterns of the recorded electron microscope images may give valuable crystallographic information regarding crystalline specimens.

3. Electron-microscope images used for optical diffraction study and the optical diffraction system

In the experiments described here, electron micrographs of labradorite feldspar taken by a JEM-100C electron microscope were used as the grating for taking the optical diffraction pattern. This instrument has recently been highly successful in high-resolution electron microscopy mainly because of the high stability of its mechanism and electronics and the small spherical aberration ($C_s = 0.7$ mm). The microscope has a point-to-point resolution of 2·5 Å and a line resolution of 0·72 Å and can give projections of the fine structure in the specimen larger than the resolution. The labradorite feldspar is the plagioclase intermediate between anorthite ($CaAl_2Si_2O_8$) and albite ($NaAlSi_3O_8$). The details of the specimen (No. 1513c) are described in the study of Hashimoto, Nissen, Ono, Kumao, Endoh & Woensdregt (1976). Since labradorite has a large unit cell (approximate cell parameters $a = 8.17$, $b = 12.87$, $c = 7.11$ Å, $\alpha = 93.6$, $\beta = 116.3$, $\gamma = 89.8°$), many Bragg-reflected waves emerge at small angles from the crystal and can contribute to the image. Therefore, much information on the specimen may be contained in the image. In most orientations chosen for micrographs of the labradorite, 50 to 100 Bragg-reflected waves pass through the aperture. Fig. 1 shows an electron-microscope image and the corresponding
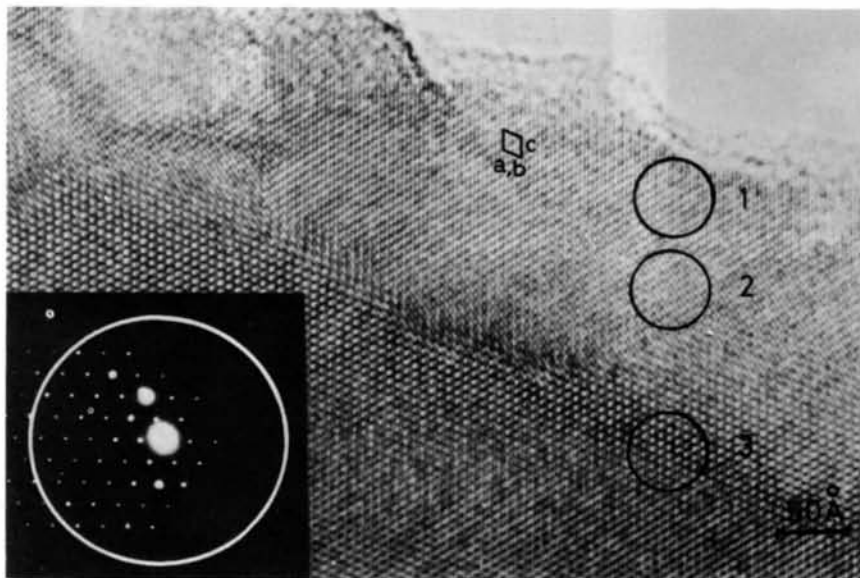

Fig. 1. Lattice image of labradorite (110) and electron diffraction pattern. Image contrasts in circles (1), (2) and (3) are very different from each other because of a thickness effect. The projected unit cell is shown within a parallelogram.

electron diffraction pattern of a thin crystal of labradorite projected on the plane almost parallel to ($1\bar{1}0$) taken at defocus $\Delta f = 1200$ Å. The size of the aperture used for taking the image is shown in the diffraction pattern. Though the electron micrograph has been produced by the interference of more than 50 waves, the optical diffraction patterns of the electron micrograph consist of fewer diffraction spots, but can show the crystallographic information stored in the electron micrograph. The size of one projected unit cell is indicated in the micrograph by a parallelogram, within which some fine structure due to the atomic arrangement is found.

The optical diffraction system used in the present experiment is shown schematically in Fig. 2. The He–Ne laser beam (6328 Å) is spread by lens $L1$ and a pinhole (50 μm in diameter), and the image of the pinhole is projected on the photographic film (film) by lens $L2$. The electron micrograph (sample) is placed between $L2$ and film. The diffraction-camera lengt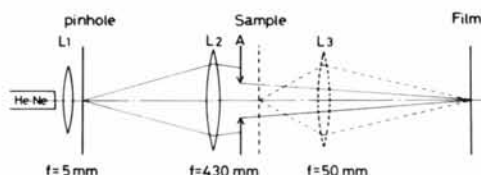h is given by the distance between sample and film. The specimen area which gives the diffraction pattern is adjusted by the irradiating beam diameter which is controlled by the iris diaphragm A. The sample is adjusted vertically and horizontally in order to select the specimen area, which is projected on the image plane by another lens $L3$ to confirm the illuminating area of the film. When the selected specimen area is too small to be selected optically by the aperture, the specimen electron micrograph is printed on a magnified scale and a suitable area is selected and again reduced photographically. The diffraction pattern from the area of a projected unit cell was taken by the procedure stated above.

4. Optical diffraction patterns of the recorded electron-microscope images

As shown already, Fig. 1 is an electron-microscope image of labradorite feldspar taken at the suitable defocus $\Delta f = 1200$ Å. The areas indicated by circles and numbers show differences of contrast which seem to be due to the thickness differences. Region No. 3 is thicker than No. 1. The optical diffraction patterns from area Nos. 1, 2 and 3 are shown in Fig. 3(1), (2) and (3). The specimen area selected for diffraction has a diameter of 80 Å and it is recorded by using the lens $L3$ shown in Fig. 2 and displayed in the lower part of Fig. 3. Both diffraction patterns and micrographs change their intensity with increasing thickness
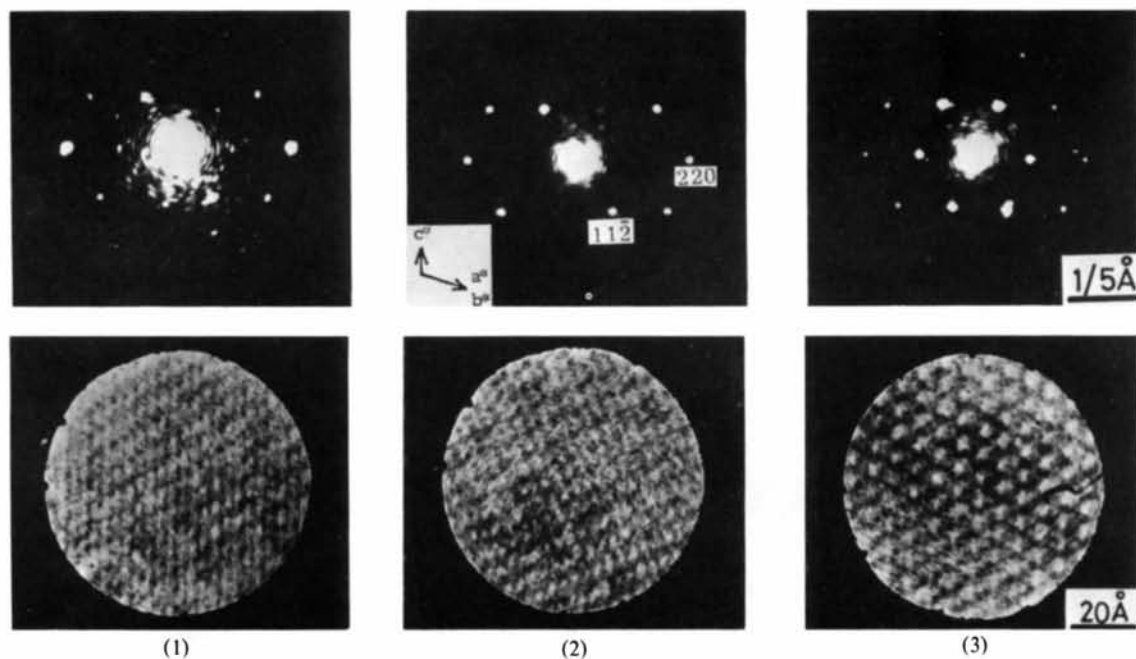
Fig. 2. Ray diagram for taking an optical diffraction pattern.

Fig. 3. Optical diffraction patterns from the areas marked (1), (2) and (3) in Fig. 1 (about 80 Å in diameter) and their enlarged images produced by lens L_3 shown in Fig. 2.

of the crystal. The 220 diffraction spot has maximum intensity in (1) and minimum intensity in (3) and the 110 spot has maximum intensity in (3) and almost no intensity in (2). Since the images were taken with the same defocus and areas Nos. 1 to 3 are in the same Bragg-reflecting condition, the intensity variations in diffraction spots and micrographs are due to the extinction effect of electron waves in the crystal, *i.e.* dynamic interaction of electron waves in the crystal. Measured spacings and angles of all optical diffraction spots have coincided with those of X-ray values (Toman & Frueh, 1973) within 2% in interplanar spacing and 2° in interplanar angles. These accuracies are sufficient for the identification of the specimen and its orientation. The intensity variation of optical diffraction spots can be explained correctly by considering the dynamic scattering of electron waves in the crystal and the image formation theory. The details will be discussed elsewhere.

It seems probable that for the thinnest regions of the crystal, such as area No. 1 in Fig. 1, the theory of §2 may give a satisfactory approximation and the diffraction intensities may be approximately kinematical (see below). It is not to be expected that these intensities will be the same as in the electron diffraction

patterns shown in Fig. 1, which is a conventional selected-area diffraction pattern obtained from a very much larger area of the crystal including some thick regions.

Fig. 4(a) is an electron micrograph of labradorite feldspar, containing a small crystal A, about 80 Å in diameter. This crystal consists of two grains marked by B and C in different orientations. Fig. 4(b) is the optical diffraction pattern from the circular area of 80 Å in diameter including the crystal A. The diffraction pattern shows clearly that the spots consist of two groups in different orientations. By reducing the aperture size of selected area to 30 Å in diameter, the diffraction patterns corresponding to each of the grains B and C were taken and are shown in Fig. 4(c) and (d) respectively. Measurement of distances and angles of the diffraction spots suggested that (110) of crystal B and (213) of crystal C are normal to the incident beam and these crystals are joined along (3$\bar{3}$1).

The selected area can be reduced to the size of a unit cell. An example of an optical diffraction pattern from the area of a projected single unit cell, whose position is indicated in Fig. 1 by a parallelogram, is shown in Fig. 5(a). The fine structure of the image of the unit cell is seen in the magnified image shown in
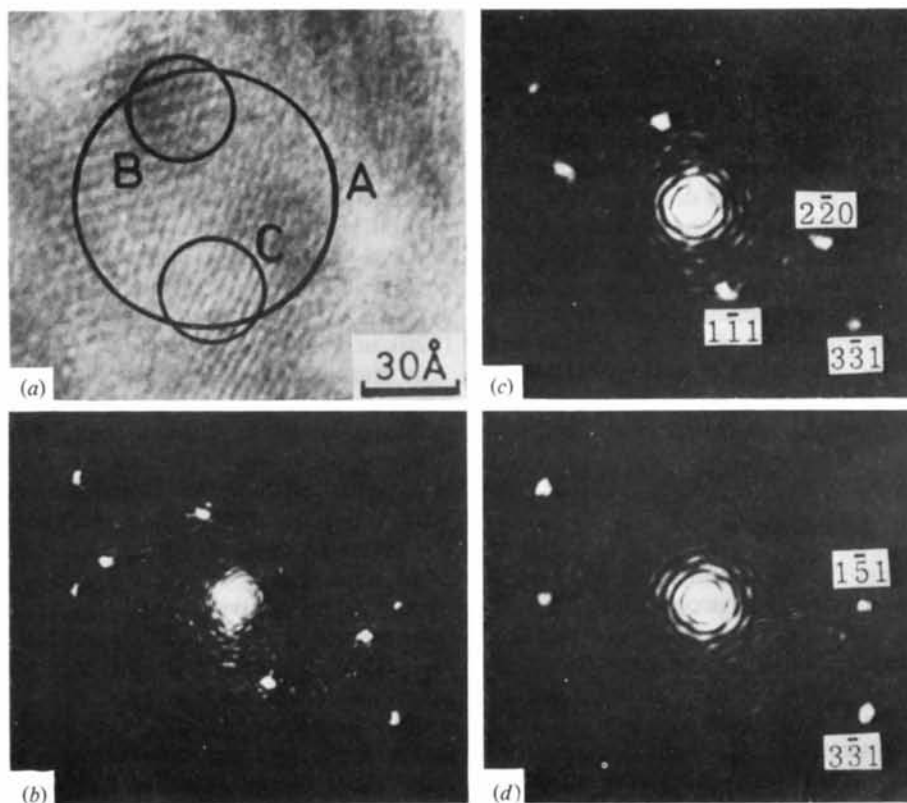

Fig. 4. Optical diffraction patterns of small crystal grains. (a) Lattice image of labradorite crystal which has some small grains. (b) Optical diffraction pattern of the central area A (about 80 Å in diameter). (c), (d) Optical diffraction patterns of crystals B and C respectively (about 30 Å in diameter).

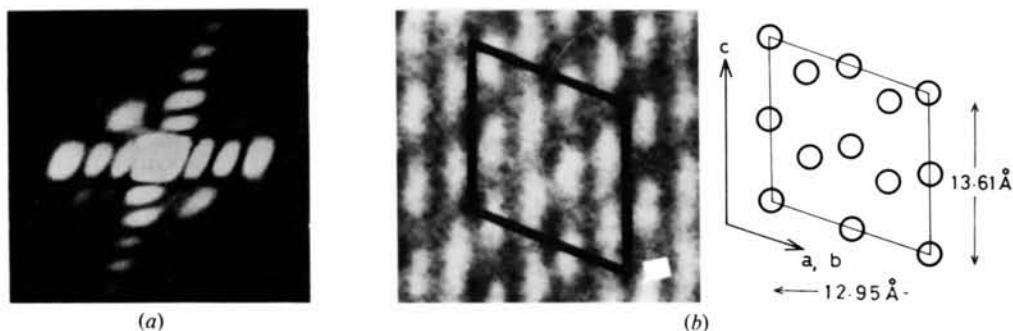(a)   (b)

Fig. 5. (a) Optical diffraction pattern of the single unit cell which is marked in Fig. 1. (b) Enlarged image of the unit cell, and corresponding sites of Ca or Na.
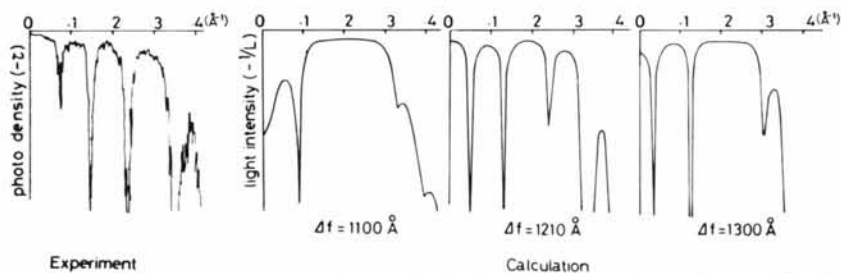

Fig. 6. Comparison of observed photographic density $-\tau$ of the optical diffraction pattern shown in Fig. 5(a) with the calculated light intensity L. Photographic density is expressed as $-1/L$.

Fig. 5(b) together with the schematic projection of non-tetrahedral atoms (Ca or Na). The intensity profile of the diffraction pattern shown in Fig. 5(a) is compared with the calculated intensity distribution which is based on the phase-grating approximation described in §2 and is shown in Fig. 6. In this calculation it is assumed that the non-tetrahedral atoms have the mean scattering amplitude of Ca and Na atoms. For the computation of the potential distribution, analytical representation of scattering factors by Smith & Burge (1962) and atomic positions by Toman & Frueh (1973) were utilized. The calculated intensity profile for the case of $\Delta f = 1210$ Å agrees with that observed.

5. Discussion

It is well known that the black and white contrast in the high-resolution electron-microscope images of very thin crystals taken under optimum conditions by using many Bragg-reflected waves shows the potential maxima and minima in the crystal, *i.e.* the positions of atoms in the crystal.

In the preceding section, it has been demonstrated theoretically and experimentally that the structure image taken at suitable focus can be used as the optical diffraction grating which gives sufficient information about the crystallographic data of the specimen crystal.

It was also demonstrated that the selected area can be reduced to the unit-cell dimension (~ 10 Å) in this condition.

The calculated error of correspondence between the specimen area selected and the area actually producing the diffraction pattern, which is expressed by $C_s \alpha^3$ becomes $11 \cdot 5$ Å for a lens of spherical aberration coefficient $C_s = 0 \cdot 7$ mm and diffraction angle $\alpha = 1 \cdot 18 \times 10^{-2}$ corresponding to $3 \cdot 14$ Å, labradorite (220), in crystal-lattice spacing.

It must be noted here that the spherical aberration which is expressed as $C_s \alpha^3$ is at the Gaussian image plane and not at the optimum focus plane.

As shown in Fig. 7, the image of a specimen point A is projected on B at the Gaussian image plane for the beam diffracted with an angle α. This is separated by $C_s \alpha^3$ from the point B', where magnification is assumed to be unity and B' is the image of a point A formed by the beam with very small diffraction angle. Therefore, the image of a point A', separated by $C_s \alpha^3$ from the point A, appears at B', if it is formed by the beam diffracted with an angle α.

If the field-limiting aperture is placed in the Gaussian image plane, and the diffraction pattern in the back-focal plane of the objective lens is projected on the second image plane by the lens $L2$ which is located behind the field-selecting aperture, the diffraction spots corresponding to the angle α not only from the area
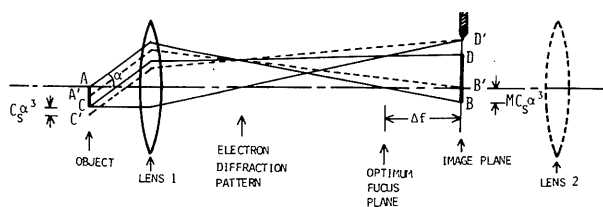
Fig. 7. Error of correspondence between the selected-image area and the area actually producing the diffraction spots. $C_s\alpha^3$, the error of selected area in the Gaussian image plane, is 1260 Å for the Al (222) plane, $\alpha = 3\cdot2 \times 10^{-2}$, $C_s = 3\cdot6$ mm, $\Delta f = 0$, and 11·5 Å for the labradorite (220) plane $\alpha = 1\cdot18 \times 10^{-2}$, $C_s = 0\cdot7$ mm, $\Delta f = 0$. $C_s\alpha^3 - \Delta f\alpha$, the error of selected area in the optimum focus plane, is $-2\cdot7$ Å for the labradorite (220) plane, $\alpha = 1\cdot18 \times 10^{-2}$, $C_s = 0\cdot7$ mm, $\Delta f = 1200$ Å.

AC, but also from $A'C'$ can be projected. Therefore, the error of correspondence between the specimen area and the diffraction pattern is equivalent to the error due to spherical aberration in the Gaussian image plane.

In the optimum focus plane, which can be obtained with the underfocus of Δf, the error in the image due to the spherical aberration is given by $(C_s\alpha^3 - \Delta f\alpha)$. For $\Delta f = 1200$ Å the error becomes $-2\cdot7$ Å, which is the accuracy of correspondence between the specimen area recorded and the area actually producing the diffraction spots.

In the process for taking the optical diffraction pattern, there is no relative shift between the specimen micrograph and the recorded pattern, and also no specimen damage such as that by electron-beam irradiation. These are useful considerations for the determination of the orientation of small crystals.

The authors would like to express their thanks to Dr H.-U. Nissen at ETH, Switzerland, for providing the labradorite feldspar specimen and for helpful discussion throughout this work, to Professor J. M.

Cowley for helpful discussion and for correcting the English, to Professor Shimizu and Mr Endoh, Osaka University, for their encouragement throughout this work, and finally to Mr A. Ono, JEOL, for his help in taking the electron-microscope images of labradorite feldspar.

References

ALLPRESS, J. G., SANDERS, J. V. & WADSLEY, A. D. (1968). *Phys. Status Solidi*, **25**, 541–550.

CLARKE, R. & THOMAS, G. (1976). *Proc. Electron Microsc. Soc. Am.* p. 492.

COWLEY, J. M. (1959). *Acta Cryst.* **12**, 367–375.

ERICKSON, H. P. & KLUG, A. (1971). *Philos. Trans. R. Soc. London Ser. B*, **261**, 105–118.

GEISS, R. H. (1975). *Appl. Phys. Lett.* **27**, 174–176.

GRONSKY, R., SINCLAIR, R. & THOMAS, G. (1976). *Proc. Electron Microsc. Soc. Am.* p. 494.

HASHIMOTO, H., NISSEN, H. U., ONO, A., KUMAO, A., ENDOH, H. & WOENSDREGT, C. F. (1976). *Electron Microscopy in Mineralogy*, edited by H.-R. WENK, pp. 332–344. Berlin: Springer.

HASHIMOTO, H., TANJI, T., ONO, A. & KUMAO, A. (1975). *J. Electron Microsc.* **24**, 212.

IIJIMA, S. (1971). *J. Appl. Phys.* **42**, 5891–5893.

IIJIMA, S. (1973). *Acta Cryst.* A**29**, 18–24.

KOIKE, H. & UENO, K. (1973). *J. Electron Microsc.* **22**, 283–284.

KOREEDA, A., OKAMOTO, H., SHIMIZU, K. & KATSUTA, T. (1971). *Rev. Sci. Instrum.* **42**, 1676–1682.

RIECKE, W. D. (1961). *Optik*, **18**, 278–293.

SCHERZER, O. (1949). *J. Appl. Phys.* **20**, 20–29.

SMITH, G. H. & BURGE, R. E. (1962). *Acta Cryst.* **15**, 182–186.

THON, F. (1966). *Proc. 6th Int. Congr. Electron Microsc. Kyoto*, pp. 23–24.

TOMAN, K. & FRUEH, A. J. (1973). *Z. Kristallogr.* **138**, 22–28.

UYEDA, R., DUPOUY, G., PERRIER, F., AYROLES, R. & BOUSQUET, A. (1963). *J. Electron Microsc.* **12**, 271.

UYEDA, N., KOBAYASHI, T., SUITO, E., HARADA, Y. & WATANABE, M. (1972). *J. Appl. Phys.* **46**, 1581–1589.

Etude Cristallographique de la Transition de Phase du Benzil

PAR GÉRARD ODOU, MARCEL MORE ET VINCENT WARIN

Equipe de Dynamique des Cristaux Moléculaires associée au CNRS (ERA 465), Université des Sciences et Techniques de Lille I, BP 36, 59650 Villeneuve d'Ascq, France

Benzil exhibits a solid–solid phase transition at $83\cdot3 < T_c < 83\cdot4$ K. The low-temperature lattice is complex triclinic: there are three kinds of domain and the space group is a pseudo-symmetry group $P321$. The lattice of each domain is triclinic, pseudo-hexagonal, with the three domains arranged around a pseudo-threefold axis.